Design study of nanograting-based surface plasmon resonance biosensor in the near-infrared wavelength

M. Tahmasebpour,[1,*] M. Bahrami,[1] and A. Asgari[2,3]

[1]Faculty of Electrical and Computer Engineering, University of Tabriz, Tabriz, Iran

[2]Research Institute for Applied Physics and Astronomy, University of Tabriz, Tabriz, Iran

[3]School of Electrical, Electronic and Computer Engineering, The University of Western Australia, Crawley, WA 6009, Australia

*Corresponding author: tahmasebpour@tabrizu.ac.ir

Received 31 October 2013; revised 19 January 2014; accepted 27 January 2014; posted 28 January 2014 (Doc. ID 200466); published 27 February 2014

A key issue with surface plasmon resonance (SPR) biosensors, which are the focus of many researchers, is improving their sensitivity to detect lower amounts of analyte in a solution. Most SPR developments have focused on the grating-based sensitivity-enhancement approach. In addition to sensitivity, a substantial enhancement of other sensor characteristics such as resolution and signal-to-noise ratio (SNR) is desired for designing a practical sensor. So, in this paper, the characteristics of surface plasmon polaritons sustained by 1D subwavelength metallic gratings on a thin metal slab (under the Krestchmann configuration) have been investigated numerically for the analyte–ligand interactions detection. Effects of different structural parameters, such as grating period, grating depth, metal film thickness, and fill factor have been evaluated on the sensor sensitivity as well as resolution and SNR. Numerical results indicate that the sensor working in the near-infrared wavelength has a better performance than that in the visible one. The result of numerical investigation has been used to design an optimized sensor with the best figure of merit. © 2014 Optical Society of America

OCIS codes: (050.6624) Subwavelength structures; (240.6680) Surface plasmons; (280.4788) Optical sensing and sensors.

http://dx.doi.org/10.1364/AO.53.001449

1. Introduction

Surface plasmon resonance (SPR) is a unique optical transduction method, which has been commercially employed for optical biosensors [1]; it is one of the most advanced label-free, real-time-detection technologies [2]. The SPR biosensors are sensitive to local refractive index changes near the metal surface and can be used to study the specificity, affinity, and kinetics of biomolecular interactions and measure the concentration levels of analytes in complex samples [3]. Special electromagnetic waves named surface plasmons (SPs), which are usually excited with incident light, are exploited in the SPR biosensors to probe changes in the refractive index at surfaces of metals. SPs are collective-free electron-density oscillations on surfaces of metals, typically gold or silver, in contact with dielectric materials [4].

In a traditional SPR biosensor configuration, known as the Krestchmann configuration, attenuated total reflection (ATR) configuration is used for excitation SPs. ATR is a phenomenon in which the impinging photons at a metal–dielectric interface, with the angle of incidence equal or greater than critical angle are totally reflected back. For angles greater than this

1559-128X/14/071449-10$15.00/0

critical angle, the light, instead of being totally internally reflected back, is coupled into the metallic film, causing a minimal reflected light intensity. This angle at which this minimum occurs is called the SPR angle, and the phenomenon arises because of oscillations of mobile surface charges [5]. These certain conditions, in which the energy carried by the photons is coupled to the SPs at a metal–dielectric interface, give rise to SPPs. This transfer of energy occurs when the momentum of the photon matches that of the plasmon [6]. To excite SPPs, which is propagating along the metal–dielectric interface, the additional momentum is required to overcome the momentum mismatch between the impinging photons and the SPPs. The most common configuration used to achieve the momentum match is the Kretschmann configuration. In the Kretschmann configuration, high-index prism is used to increase the momentum of the incident photons and excite propagating SPs along the metal–dielectric interface [7].

The SPPs excited are strongly localized across the interface and may be considered classically as electromagnetic (EM) surface waves propagating along the metal–dielectric interface and decay exponentially with distance normal to the interface. Since SP waves are tightly bound to the metal-dielectric interfaces penetrating around 10 nm into the metal (the so-called skin depth) and typically between 100 and 600 nm (for the wavelengths in the visible and near infrared) into the dielectric, they concentrate EM waves in a region that is considerably smaller than their wavelength [8,9]. This propagating SPR (PSPR) is considered as more classical since it has been known for a longer time. Another type of SP is the localized surface plasmon resonance (LSPR), which could be the basis for biosensors of comparable or even better performance. The localized SPPs (LSPP) are free-electron-density oscillations in metallic nanostructures coupled with confined electromagnetic fields and can be excited by tuning the excitation optical frequency to the LSPP resonance frequency where energy transfers happen between impinging photons and LSPPs [4]. They are excited in metallic structures with lateral dimensions less than the wavelength of the exciting EM wave [10]. Useful characteristics of metallic nanostructures include local field enhancement and metamaterial-like behavior. Sensitivity can be increased by increasing the surface area, and local field enhancement occurs at nanostructures [11]. So the extremely intense and highly localized EM fields induced by LSPR make these sensors highly sensitive transducers of small changes in the local refractive index [10]. On the other hand, the latest advancements in nanotechnology have made feasible the fabrication of structures with nanometer-scale features; thus metal nanostructures have received considerable attention for their ability to guide and manipulate light (SPPs) at the nanoscale [12].

Among the metal nanostructures, surface-relief nanostructures can be used to create LSPs. In contrast to using nanoparticles to excite localized plasmons, surface relief patterns have advantages of no aggregation and precise control over the device geometry; thus they offer reliable sensing performance [13,14]. In a Kretschmann-configuration-based SPR sensor, metallic nanograting as a surface relief pattern has been widely utilized to further improve the sensor performance. Note that the presence of metallic grating can improve the sensor performance because of localized surface plasmon (LSP) excitations with strongly enhanced field intensity and sensitivity enhancement by an increase of surface reaction area, which mediates additional interactions between excited plasmons and local binding events [12,15–17]. Moreover, nanograting SPR sensors have a simple structure for mass fabrication. Recent developments in nanolithography and nanofabrication methods can make it possible to fabricate these sensor chips at low cost in mass manufacturing [2,18]. Thus nanograting SPR sensors can be used as an economic tool for high throughput screening application [16].

Among the reported articles on SPRBs using periodic nanograting, a sensitivity-enhancement approach was presented using a nanowire-based SPR structure [17]. In that study, the structural dependence of the SPRB on nanowire design parameters, particularly the volume factors and nanowire depth and also on the sensitivity characteristics, was emphasized. An optimization for the optimal nanowire structure was also carried out by using a numerical model for the rigorous coupled wave analysis (RCWA) as well as the FDTD method. However, a detailed discussion on the resolution, which is related to the sharpness of the reflectance curve, was not tackled. In a recent study, the nanowire structure was utilized for the SPR imaging, and it has been verified that the nanowire structure can equally be employed for the sensitivity enhancement of the SPR imaging and nonimaging of the angle interrogation type SPRBs [19]. Although in this study an optimum grating structure for the SPR imaging was investigated based on maximizing reflectance sensitivity enhancement factor, no discussion on the detection accuracy was given. Such a nanowire-based sensitivity enhancement in SPRBs and its nanofabrication techniques has been reported in experimental studies [18,20,21]. However, most studies on SPRBs are based on numerical simulations. In another recent study, it has been reported that employing the dielectric subwavelength gratings in SPRB significantly improves the sensitivity. Also a numerical investigation for structural parameters has been described to optimize the SPRB using RCWA and FDTD analysis. In that study, it was demonstrated that the figure of merit (FOM) of the dielectric grating-based SPR system could be better than that of an optimized metallic grating structure [22]. But a detailed description of the detection accuracy of the metallic grating was not presented.

Much of the studies about nanograting-based SPRBs address sensitivity enhancement, but a substantial discussion on the detection accuracy has not been covered in the articles. Although sensitivity enhancement is a benefit of using metallic nanograting in SPR biosensing applications, there is a trade-off between sensitivity and detection accuracy. So for designing a practical SPRB, it is necessary to enhance detection accuracy as well as sensitivity. Moreover, the properties of the grating-based SPRBs were often studied in the visible wavelength of 633 nm. Since in the near-infrared (NIR) regime, SPR offers high probe depth [11] and more precise determination of SPR dips [23], it is important to realize a nanograting-based LSPR sensor for the NIR regime.

In this paper, the SPR in 1D rectangular-like geometry nanostructure film under the Krestchmann configuration is investigated for NIR wavelength using the finite element method (FEM) as a numerical simulation method. Since a large number of structural parameters are involved in the design of the nanograting-based LSPR biosensor, a comprehensive numerical analysis was carried out to investigate the effect of the design parameters, including grating depth, grating period, and fill factor. The optimization of nanograting geometry based on maximizing the parameter of FOM in the NIR wavelength is carried out for first time. Additionally, influence of the flat metal layer thickness on the SPR characteristics is investigated and considered in the optimization, which is not performed in the majority of previous studies. The numerical results indicate that the sensor with higher FOM can be achieved in the NIR wavelength even contrary with dielectric grating LSPR sensor, which is presented in [22].

2. Design Consideration and Theoretical Model

A. Model and Simulation Methods

Figure 1 shows a schematic diagram of ATR for generation of SPs with a rectangular-like metal nanograting structure placed on top of an intermediate metal layer. The sensor is considered as a reflection-type plasmon-based biosensor, which reflected light measurement by a photodetector in the same side of the incident light allows an extremely compact biosensing scheme. In the diagram, dg represents the height of the metal grating, and dm is the intermediate metal layer thickness. The metal nanograting structure has the period of P. The width, w, indicates the part of grating that is filled with metal and used for defining fill factor. The fill factor (f.f) is the ratio of w over the period (w/P). High-index glass with the refractive index of n_p is used as the substrate and also as the coupling device, which is similar to the standard Krestchmann SPR setup. Although different metal materials are used for metallic films and surface relief nanostructures, gold is the most popular material because of its excellent biocompatibility and wide availability of linker molecules [13]. Thus Au is considered the material of the

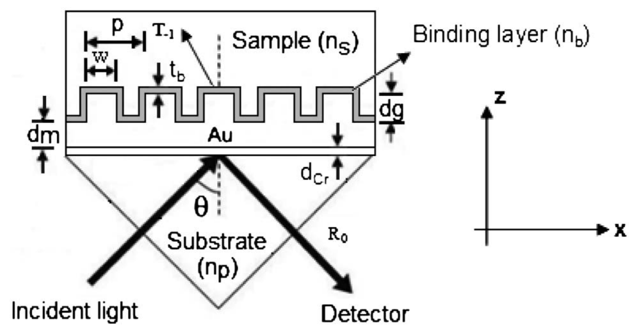

Fig. 1. Proposed model for nanostructured SPR sensor.

nanograting structure and metal film in this work. The gold film is coated on the prism via an attachment of a 2 nm thick chromium layer, which is indicated by d_{Cr} in Fig. 1. The sensing operation of the proposed nanograting-based SPRB is observed through monitoring the binding of the DNA hybridization. The DNA hybridization is modeled as a 2 nm thick dielectric layer that covers the whole sensor surface and is shown by t_b in Fig. 1. DNA size can be thicker than 2 nm for experimental applications. By assuming 2 nm thick for our study, the worst-case sensitivity data in the calculation of the sensitivity enhancement has been taken [17]. The refractive index of the binding layer (n_b) is set to be 1.40 for DNA ligand immobilization, and this value increases up to 1.50 with the interaction between capture and target probes [22]. The biological sample (analyte) in the nanoslits and below is considered as the phosphate buffered saline (PBS) solution, which is assumed as a dielectric material with the refractive index n_s equals to 1.33 [22].

For the proposed structure, the incident light can illuminate the backside of the metal film under total internal reflection condition, giving rise to evanescent light. The evanescent light penetrates the metal film and reaches the surface of the metal grating. The wave number of the evanescent light incident on the grating surface at angle θ is given by the following expression [6]:

$$K_0 = \frac{2\pi}{\lambda}\sqrt{\varepsilon_p}\,\sin\theta, \tag{1}$$

where ε_p is the dielectric constant of the prism and λ is the incident light wavelength. When TM-polarized light is incident on the prism, the dispersion relation of the excited SPs at resonance conditions is determined by the following equation [6]:

$$K_{\mathrm{SPR}} = K_0\sqrt{\frac{\varepsilon_{D,\mathrm{eff}}\varepsilon_{AU}}{\varepsilon_{D,\mathrm{eff}}+\varepsilon_{AU}}}, \tag{2}$$

where K_0 and K_{SPR} denote the wave vectors of the incident light and SP, respectively. $\varepsilon_{D,\mathrm{eff}}$ is the effective permittivity of grating layer in combination of surrounding dielectric analytes. ε_{AU} is the dielectric constant of the gold film. The evanescent light is diffracted by the grating, and this diffraction increases the wave number of the evanescent light in the x direction by qK, where K is the magnitude of the wave vector of diffracted light and equals to $2\pi/P$, and q is the diffraction order. When the light is incident on the grating surface with angle θ, the wave number of the qth diffracted evanescent light is given by the following equation:

$$K_q = K_0 + qK, \qquad q = 0, \pm1, \pm2, \pm3, \ldots. \tag{3}$$

Therefore the incident light is coupled with the SPR whenever the wave numbers of the diffracted evanescent light and the SP satisfy the following condition [24]:

$$K_q = \pm K_{\mathrm{SPR}}. \tag{4}$$

The sign of K_{SPR} can be determined by q. The expressed equations above were used to calculate SPR curves with considering higher diffraction orders in the proposed device configuration. The transmitted negative first order is shown schematically in Fig. 1.

The numerical technique used for calculating the reflectance and transmittance from the nanograting metal film is FEM [25–28]. The dispersion curve of the sensor is calculated numerically for TM-polarized light in a broad wavelength range of 400–1500 nm. SF10 glass substrate with dispersive index refraction is used as a prism. All optical parameters of metals and substrate are taken from [29]. The design parameters, such as grating period, grating height, metal film thickness, and fill factor are included in the simulation to analyze the sensor-performance parameters. Optimal structure parameters for NIR wavelength of 984 nm were calculated by using algorithms based on the FEM analysis of the proposed structure. The validity of this numerical method has been verified with comparing the result with the standard electromagnetic field calculation using Fresnel equations and the matrix formalism [14,30,31].

B. Sensing Performance of the Proposed Structure

It has been well known that use of metallic nanostructures on a SPR biosensor leads to fairly obvious sensitivity improvement in comparison with a conventional one, but other obtained LSPR characteristics become far from desired. The sensitivity enhancement in the event of a strong LSPR is often accompanied by a broad and shallow SPR dip in the reflectance curve [32].

In general, the performance of any SPR sensor is determined in terms of three aspects. The first is sensitivity (S), which is defined as the ratio of the SPR angle shift due to the refractive index change in sensing layer. Higher sensitivity corresponding to the relation of LOD $= \sigma/S$, where σ is the standard deviation of noise of the sensor signal, improves the limit of detection (LOD) or resolution of the sensor. Thus it should be as large as possible in SPR biosensing applications in order to monitor tiny biomolecular interactions quantitatively and accurately [33,34]. Second, FWHM corresponds to the SPR curves, which should be as small as possible. The accuracy of the detection of the SPR resonance angle is dependent on the width of the response curve in the reflectivity. This indicates that high detection accuracy results from narrower FWHM, which in turn helps in accurate measurement of resonance angle [23]. Third, the minimum reflectance at resonance (MRR), which is a measure of the signal contrast of SPR curve (i.e., signal-to-noise ratio) and should be as deep as possible. The MRR indicates an intensity of incident beam converted into SPs, and thus a deeper MRR would be desired for a larger excitation of SP waves.

In order to improve sensitivity, SNR, and resolution of the sensor, we also need the resonance curve in the spectrum of the output signal represents a high displacement, small bandwidth, and deep depth to allow precise analysis of sensing events [22]. Subsequently the LSPR sensor overall performance can be evaluated by employing parameter of FOM, which is defined as follows [22]:

$$\mathrm{FOM} = \frac{S}{\mathrm{FWHM}}(1 - \mathrm{MRR}). \tag{5}$$

3. Calculation Results and Discussion

A. Electrical Field Distribution on the Surface of Nanograting

As is well known, existence of metallic grating induces the electromagnetic field localizing on the surface of the grating, whereas the sharp edges have the strongest value of the EM field. Figure 2 shows that

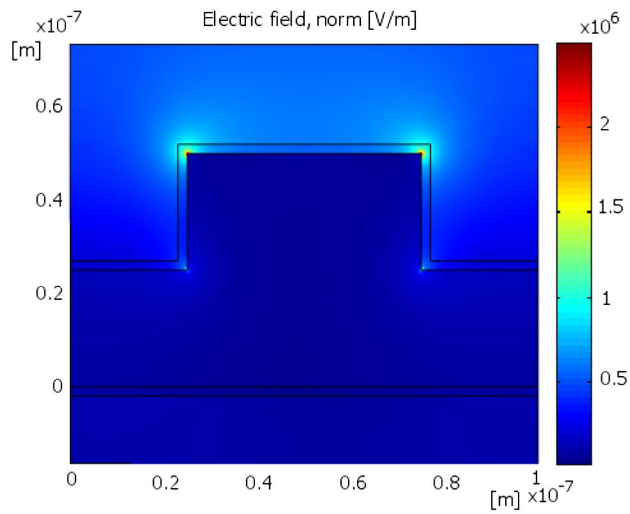

Fig. 2. Electrical field distribution on the grating surface for initial parameters of dm = 25 nm, dg = 25 nm, f.f = 0.5, P = 100 nm, and $\lambda = 984$ nm.

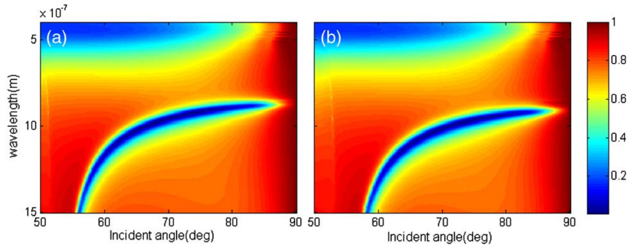

Fig. 3. Movement of dispersion curve with bulk refractive index variation from (a) ns = 1.33 to (b) ns = 1.36 (dm = 40 nm, dg = 40 nm, f.f = 0.5, P = 100 nm).

the maximal local field intensity exists at the grating edges for the NIR wavelength of 984 nm. As mentioned, penetration depth of the NIR wavelength is higher than a visible one, which allows detection of thicker targets.

Compared with a conventional SPR detection system, periodic metallic nanostructures built on a thin metal film could serve as an effective way to generate a locally enhanced field by a resonant excitation of LSP modes [22]. Excitations and decoupling of bulk SPPs and LSPs in gold nanowires typically generate hot spots around nanosized metallic structures and also lead to a significant sensitivity gain [19]. Since the parameter of dg is an indicator of interactions between LSPs and bulk SPs, a LSP is well isolated from bulk SPs in thick gratings. Thus it is possible to design a high sensitive LSPR sensor with a high grating thickness selection.

B. Dispersion Curve Characteristics for Different Grating Height and Period of the Proposed Structure

Angle-dependent reflectivity reveals dispersion characteristics of plasmonic modes when SPs are excited. SPs position in a dispersion diagram, indicated by regions with minimum reflectivity, can be displaced due to the sample or a monolayer refractive index change. As shown in Fig. 3, location of the dispersion curve is moved in a diagonal path down and to the right toward larger angles and longer wavelengths when the sample index increases from 1.33 to 1.36. It is clear that, when the refractive index change occurs only in a monolayer, the sensitivity will be reduced [35]. Such a movement allows us to measure refractive index change in dielectric material surrounding the grating through wavelength or angle interrogation approaches. It is demonstrated that angle interrogation can lead to higher sensitivities in comparison with a wavelength one [35].

Moreover, position of the resonance dips in the dispersion curve can be controlled by manipulation of grating structural parameters, such as grating thickness and period. Dispersion curves of the proposed sensor for a small grating period of 50 nm and three different values of grating thickness equals 5, 15, and 45 nm, as indicated in Fig. 4. Also plotted in Fig. 4(a), the dispersion curve for a thinner grating depth of 5 nm is not distributed so much; it is same as the conventional SPR sensor dispersion curve. Figure 4(b) indicates that increasing dg similar to the sample refractive index increase moves dispersion curve in a diagonal path down. Figure 4(c) shows that this movement increases for thicker gratings whereas in the case of the gratings, thickness equals 45 nm upper edge of dispersion curve crosses over the wavelength of 1000 nm. As plotted in Fig. 4(c), no SPR mode is excited in the visible wavelengths for a grating thickness of 45 nm and small grating period of 50 nm, though the location of dispersion curve is displaced by the grating period.

In the case of the reflection-type SPR sensors that do not outcouple a radiation mode, it is necessary to consider a certain limit for P to avoid higher diffraction orders production [14]. If the grating period is sufficiently small, no diffraction orders exist above the grating. Only the near fields of the grating are present. In the case of larger grating constants, in addition to the near fields one or more grating orders exist as well and lead to interferences with the exciting evanescent field and thus reduced the enhancement of the SPs [12]. In addition, the coupling between the LSP modes is weakened for large grating periods, and, consequently, the enhancement of the SPs becomes weak [22]. Also a decrease in P

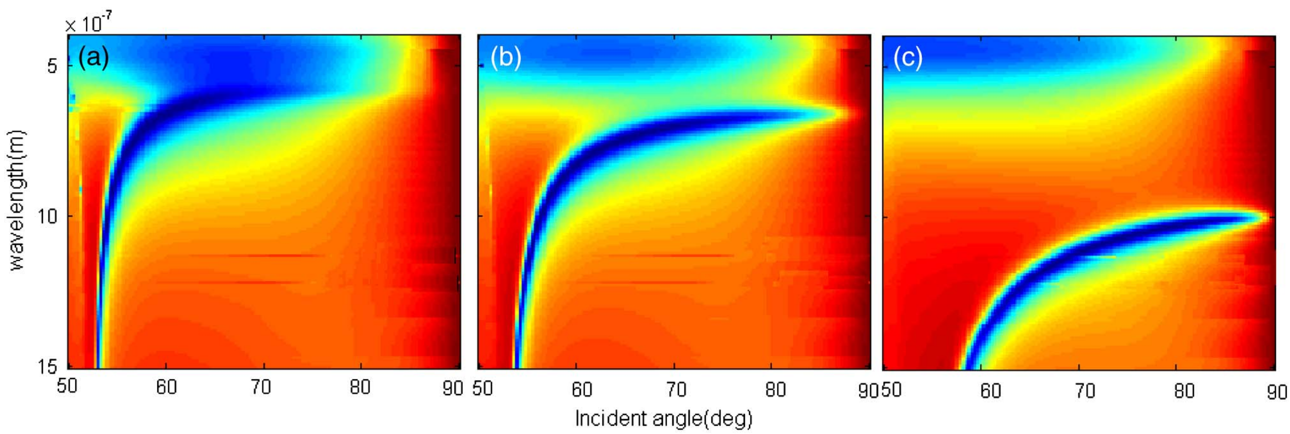

Fig. 4. Displacement of dispersion curve with grating thickness variation (a) dg = 5 nm, (b) dg = 15 nm, and (c) dg = 45 nm (dm = 40 nm, f.f = 0.5, P = 50 nm).

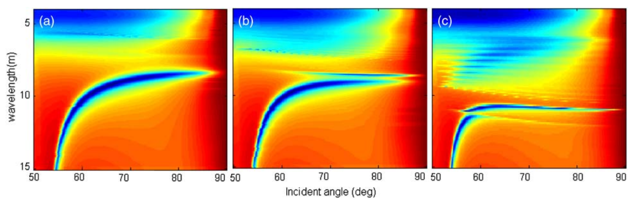

Fig. 5. Displacement of dispersion curve with grating thickness variation: (a) P = 200 nm, (b) P = 250 nm, and (c) P = 350 nm (dm = 40 nm, dg = 40 nm, f.f = 0.5).

can lead to an increase in the volume of the grating, which induces a stronger coupling of the SPs.

Moreover, it has been demonstrated that when −1 reflected diffraction occurs in periodic structures, the propagation of SP is blocked due to Bragg reflection, which occurs when the grating period equals to half of the periodicity of SP wave. This phenomenon creates energy gaps in the dispersion relation of the SP. The plasmonic dispersion curve is flat on the edge of the bandgap. This is a recurrent phenomenon in most bandgap situations. It has described that operating near the bandgap is more sensitive [35]. Dispersion curves for different grating periods are plotted in Fig. 5. As shown for P values smaller than 250 nm, higher diffraction orders can be neglected whereas for P values larger than 250 nm higher diffraction orders are produced. Figure 5(c) shows that the bandgap observed clearly for P equals 350 nm due to the generation of −1 reflected diffraction order. Location of the bandgap can be controlled with adjusting the value of P and dg. Consequently, larger values of dg for an increasing localized electrical field and values of P smaller than a certain limit for neglecting of higher diffraction orders are desired in reflection-type SPRBs.

Numerical results of angle interrogation characteristics, including sensitivity and reflectivity for broad wavelength range from visible to NIR, are indicated in Fig. 6. A large value of grating thickness equals 40 nm, and grating periods up to 250 nm are considered in the calculation. Performance of the sensor is studied for bulk refractive index variation from 1.33 to 1.36. As mentioned, the result of this numerical study can be used for monolayer refractive index sensing.

Figure 6(a) shows that, as expected, for higher value of P equals 250 nm, a bandgap region is generated, which is observable from the reflectivity curve in the wavelength range from 860 to 920 nm. Near this created bandgap, sensitivity is high; though resulted sensitivity is higher than that in the case of smaller grating periods, which do not induce production of any higher diffraction orders. The highest sensitivity is related to the period of 50 nm with approximately 300 deg/RIU sensitivity. This high sensitivity occurs in vicinity of the NIR wavelength of 980 nm, which is related to the edge location of dispersion curve, which is presented in Fig. 6(b). As observed in Fig. 4, the dispersion curve shifts toward shorter wavelengths for thinner grating heights. Thus, decreasing grating thickness

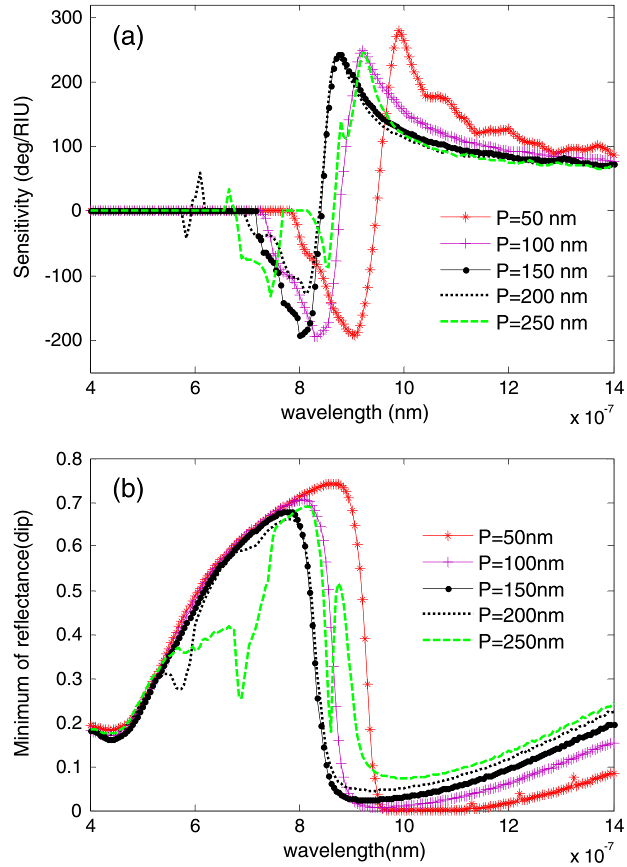

Fig. 6. (a) Sensitivity and (b) minimum of reflectance of the angle-interrogated SPR sensor with wavelength and grating period variations (dm = 40 nm, dg = 40 nm, f.f = 0.5).

will shift the sensitivity curve collection, presented in Fig. 6(a), with decreased amplitudes toward shorter wavelengths. Increasing the thickness and decreasing the period of the grating has been used as effective ways to enhance the sensitivity [22]. The growth of the sensitivity with these approaches is due to the fact that the overall surface reaction area, which could provide more room for target analytes attached to the sensor substrate, increases. On the other hand, the excitations of the SPs are strongly influenced by the grating period. Thus the period of grating is required to be kept small to obtain maximum sensitivity while maintaining the other parameters optimum.

C. Effect of Metal Film Thickness and Grating Height on Sensor Performance

Our numerical study, which optimized sensitivity for the proposed sensor, can be obtained from the grating period and operating wavelength of 50 and 980 nm, respectively. Effects of other structural parameters on the sensor performance are studied numerically for DNA hybridization detection using a laser in the wavelength of 984 nm and grating period of 50 nm.

The effects of dg variation from 5 to 40 nm and dm from 15 to 60 nm on the reflectance curve characteristics and the maximum electrical field intensity obtained at the grating surface have been plotted in

Figs. 7(a)–7(f). The reflectance curve is obtained from FEM calculations using a proposed model, as the light incidence is scanned with an angular resolution of 0.01°. The initial parameter of f.f is considered 0.5.

Figure 7(f) shows that the maximum electrical field intensity at the grating surface is increasing with increasing dg, which means the electrical field is localized stronger on the surface of thicker gratings. As a result of increased field localization for thicker gratings, the sensitivity is increased, as shown in Fig. 7(a). Also a strong dependence of the sensitivity on dg is obvious.

Figures 7(b) and 7(c) show the broadening of an SPR curve and deterioration of sensing contrast of SPR detection system, respectively, for thicker gratings. Also Fig. 7(e) indicates that as dg increases from 5 to 40 nm with a step of 5 nm, the resonance angle tends to increase gradually from 55 to 75 because the growing dg causes a local refractive index surrounding the metal film to be effectively increased. Strongly excited LSP modes in larger dg occur at an increased resonance angle. This indicates that the perturbation introduced by the nanowires modifies strongly the SPPs in the gold film. In other

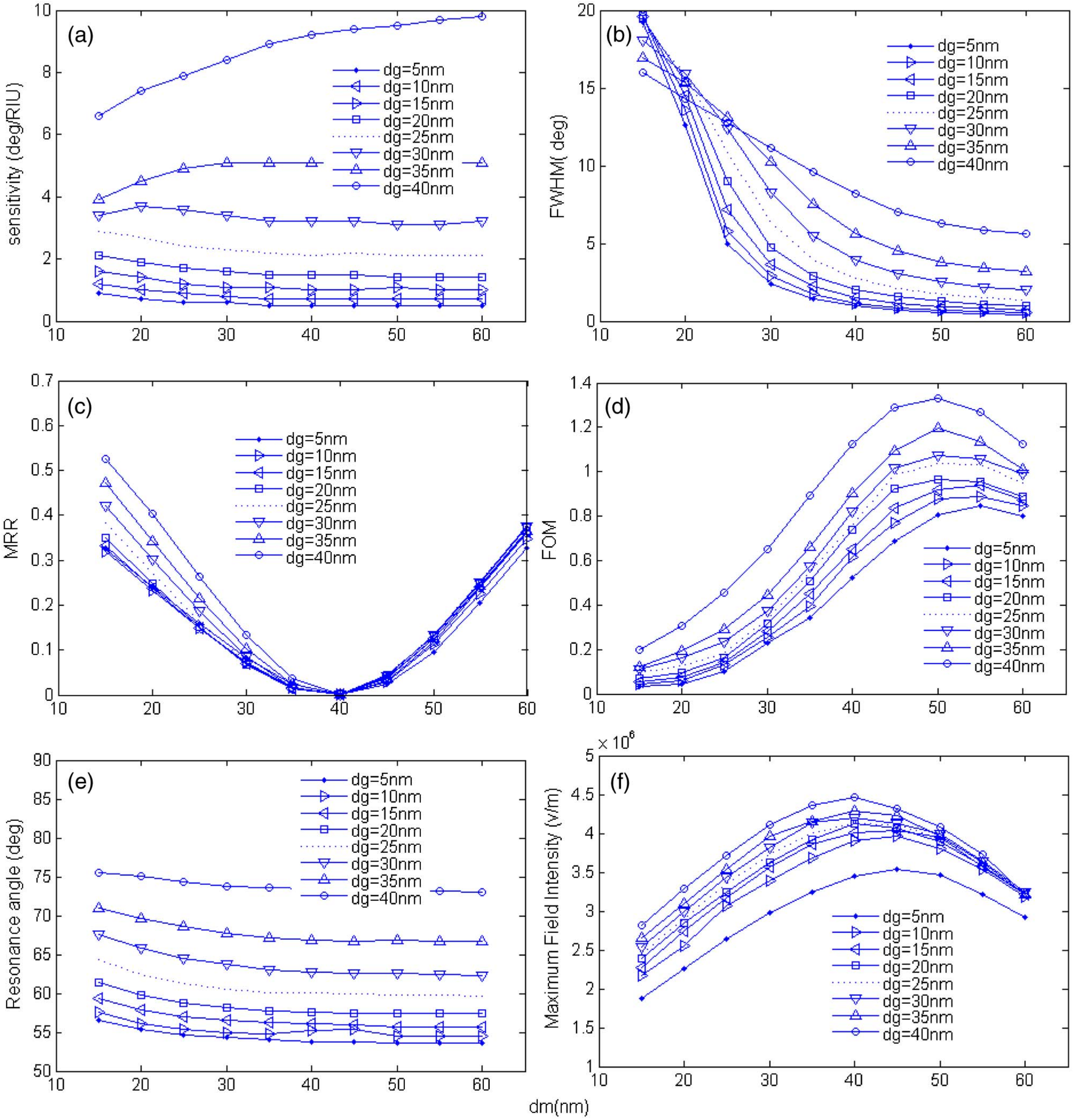

Fig. 7. Variation of dm and dg effect on the sensor performance (f.f = 0.5, P = 50 nm): (a) sensitivity, (b) FWHM, (c) reflectance minimum (dip), (d) FOM, (e) resonance angle, and (f) maximum of $|E|^2$ on the nanograting surface.

words, the momentum matching is achieved at a higher wave number; thus much higher energy is needed to excite an LSP mode.

Also Figs. 7(a)–7(f) show the effect of dm variation on the SPR characteristics. As shown, dm has an insignificant influence on the sensitivity and resonance angle. On the other hand, influence of that on the FWHM and MRR is more than the effect of dg. Bandwidth of the reflectance curve is sharper if the metal film thickness is increased. This sharper SPR curve is probably due to the smaller SP propagation attenuation along the nanostructured metal film for thicker flat metal films. In contrast to thick metal films, thin ones increase the loss of the propagating evanescent wave, reducing its propagation length, resulting in a broad resonance response. These results show that the variation in the flat metal film thickness slightly changes the SPR curve with the same trend as in the uniform metal film [6]. As shown in Fig. 7(f), and similar to the planar metal film structure, there is a metal film thickness in which maximum energy of the incident photons is converted to the plasmon energy, causing a dip in the reflectivity curve; correspondingly, the strongest electric field on the grating surface occurs on that thickness. On the other hand, it has been confirmed that for practical applications in biosensing, maintained MRR has to be smaller than a reference threshold value [17]. In this work, it is assumed to be 0.03 similar to that reported in [17]. It is clear from Fig. 7(c) that the best choice for dm is 40 nm, which leads to a minimum dip smaller than 0.002 for all values of dg varying from 5 to 40 nm. In case of other values of dm, the value of MRR is increased by variation of dg.

As shown in Fig. 7(d), the overall performance of the sensor, which is determined with the parameter of FOM, has a maximum value of 1.3. But if the reference threshold value of MRR is set to 0.03, the best value of FOM is 1.12, which is related to the case of dm = 40 nm and dg = 40 nm. As a consequence, an optimum nanograting height exists, although the optimum may depend on other parameters, such as f.f and P.

D. Effect of Fill Factor on Sensor Performance

The effect of the f.f parameter on the sensor performance is shown in Figs. 8(a)–8(f). The numerical simulations show that the SPR characteristics are significantly influenced by the f.f variations, especially in the case of the thicker gratings. Figure 8(f) indicates that the peak of maximum field intensity obtained on the grating surface occurs in two different modes of enhancement at a small or large value of f.f. In the case of low f.f, the slits are wide, and field enhancement due to the LSPR is associated with single nanograting corrugates. But in high f.f, in which slits become narrower, the field enhancement is associated with the resonant coupling of LSPs through nanogrooves. Note that the LSP excitation associated with a nanogroove tends to be noticeably stronger than that of a single nanowire [19]. These two LSP excitation modes can be coupled with effective LSPR enhancement in the case of higher grating thickness and lower grating periods. In other words, LSPR enhancement is reduced if the coupling between the two modes is weakened for a small grating thickness and large nanograting periods. At a very small period and high f.f, it is apparent that the two modes of enhancement begin to merge and create significant coupling of LSPs excited in neighboring nanowires.

Figure 8(a) shows that maximal sensitivity enhancement is achieved near two mentioned f.f due to the strong LSPR enhancement near them. As presented in Fig. 8(a) and similar to other researcher's findings [17], the sensitivity can be negative if the resonance angle shifts lower as a result of surface modification by biomolecular interactions or structural changes in a LSPR based biosensor.

It has been known that when the excitation of LSP modes are dominant, large SPP damping is observed, as it makes SPR curves broader and shallower and also induces the resonance at higher angle [32]. As observed in Figs. 8(b) and 8(e), FWHM and resonance angle of the reflectance curves are increased in the case of field enhancement near low and high f.f. Also Fig. 8(d) shows the MRRs are largely increased, as LSP modes in nanowires are excited near two mentioned f.f. The numerical results are used to evaluate the FOM parameter of the sensor. As shown in Fig. 8(c), the maximum value of FOM is obtained near high f.f. The resulting maximum FOMs are abstracted in Table 1 for different grating thickness varying from 20 to 40 nm, which leads to sensitivities larger than 10 deg/RIU.

The results therein can be used to optimize the structural parameters of the sensor. This indicates the existence of an optimum FOM, which is equals 5.9 for a structure with parameters of dg = 25 nm, P = 50 nm, and f.f = 0.9. The obtained sensitivity increase for such an optimum structure exceeds magnitude 99.5 deg/RIU. This FOM is larger than that obtained in a recent study, which was performed on both a dielectric and metal-grating-based SPR biosensor in a visible wavelength of 633 nm [22]. As mentioned in that study, FWHM and MRR of the SPR curves are not significantly influenced by the growing grating thickness in a dielectric grating, but sensitivity saturates for higher grating thickness values. Our simulation results about dielectric-grating-based SPRB corresponding with their reported results show that the parameter of FOM is restricted to the value of 2 due to the value of 10 deg/RIU sensitivity saturation. In addition, in that study the parameter of FOM for an optimized metal grating structure with dg = 5 nm was reported 1.12 in the visible wavelength of 633 nm. Moreover, our result for metal grating optimization is in line with the optimized structure with reported parameters of f.f = 0.78, dg = 20 nm, P = 50 nm in [17], which is performed on the base of maximizing

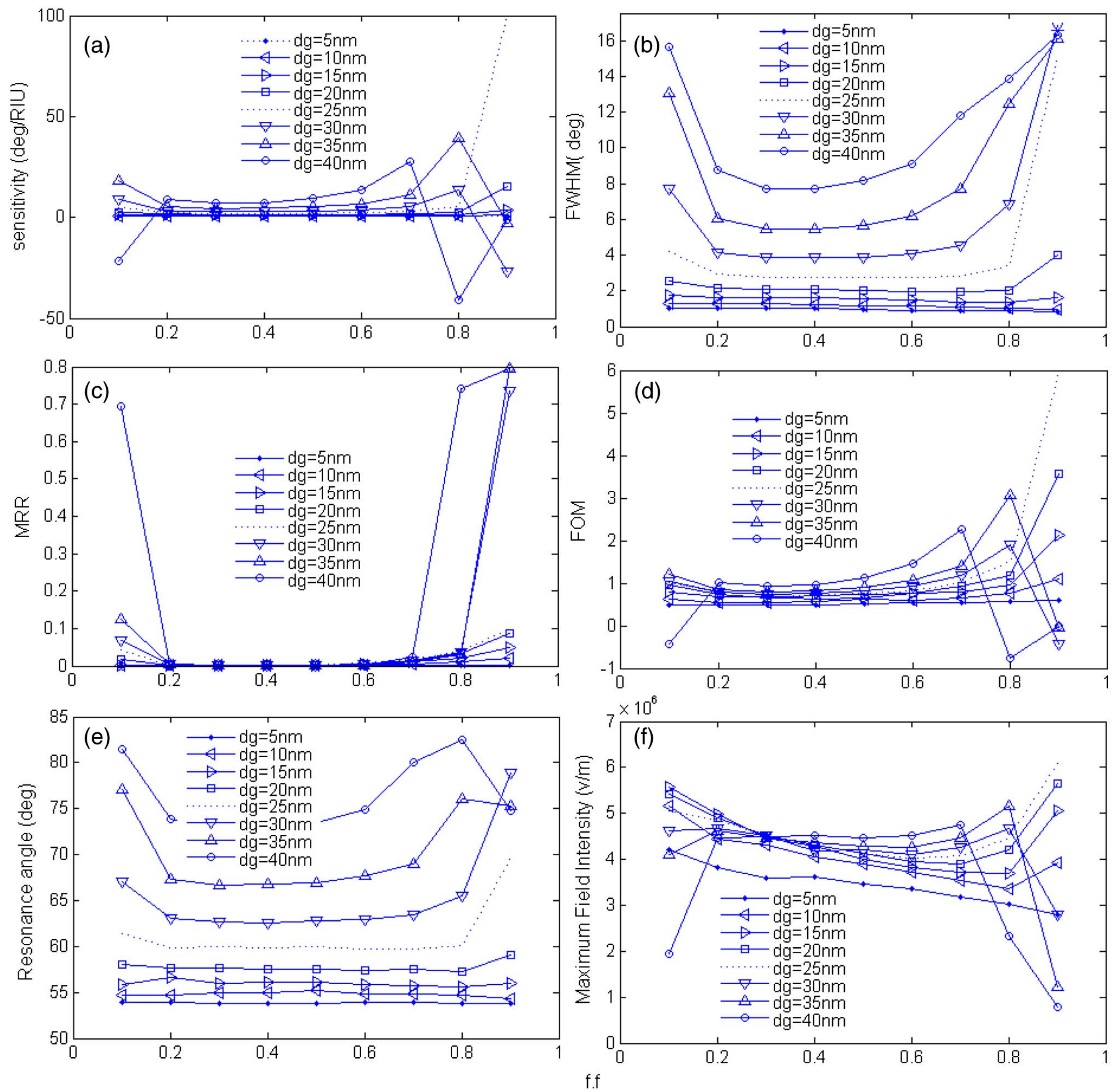

Fig. 8. Variation of fill factor effect on the sensor performance (dm = 40 nm, P = 50 nm): (a) sensitivity, (b) FWHM, (c) FOM, (d) resonance angle, (e) reflectance minimum (dip), and (f) maximum of $|E|^2$ on the nanograting surface.

the ratio of sensitivity to MRR and resulted to MRR of 3.38% and sensitivity of 23.64 deg/RIU.

Finally, our numerical results summarized in Table 1 show that the optimized structure in case of MRR ≤ 0.03 has an f.f parameter of 0.8 in line with the reported f.f value of 0.78, and the sensitivity of 39.6 deg/RIU is better than the reported value of 23.64 deg/RIU in [17]. Note that despite a

Table 1. Summary of the Sensor Performance and Optimization Calculation

Dg (nm)	dm (nm)	f.f	P (nm)	S (deg/RIU)	FWHM (deg)	FOM	Maximum Field Intensity (v/m)	Resonance Angle (deg) with DNA Hybridization	MRR
20	40	0.9	50	15.6	4	3.5	5.63e + 06	60.17	0.0858
25	40	0.9	50	99.5	15	5.9	6.08e + 6	79.5	0.0986
30	40	0.8	50	13.5	6.85	1.9	4.7e + 6	66.8	0.0359
35	40	0.8	50	39.6	12.48	3	5.16e + 6	79.98	0.0312
40	40	0.7	50	27.5	11.82	2.27	4.76e + 6	80.1	0.0234

somewhat arbitrary choice of threshold MRR being 0.1 or 0.03 in the optimization process, the FOM and sensitivity are enhanced from the reported values about the metal and dielectric gratings in [17,22].

4. Conclusion

In this paper, the surface plasmon resonance behavior in nanostructured metal film under Krestchmann configuration for biosensor application was demonstrated. The characteristics of the sensor for the structure were calculated numerically. Also, the effect of geometry parameters variation, such as grating height, metal film thickness, fill factor, and the period of the 1D nanostructured gold metal films on the sensing performance have been studied. It was demonstrated that the proposed SPRB provides better performance in terms of sensitivity and FOM in NIR wavelength compared to the ones in the visible wavelength. Finally, the optimization of the sensor geometry parameters was performed to have a sensor with the best effective figure of merit. The findings in this work can be potentially useful for designing better and optimized nanostructured metal film SPR biochemical sensors in an NIR wavelength.

References

1. S. S. Y. J. Homola and G. Gauglitz, "Surface plasmon resonance sensors: review," Sens. Actuators B **54**, 3–15 (1999).
2. A. Abbas, M. J. Linman, and Q. Cheng, "New trends in instrumental design for surface plasmon resonance-based biosensors," Biosens. Bioelectron. **26**, 1815–1824 (2011).
3. M. A. Cooper, *Label-Free Biosensors Techniques and Applications*, 1st ed. (Cambridge University, 2009).
4. H.-S. Leong, J. Guo, R. G. Lindquist, and Q. H. Liu, "Surface plasmon resonance in nanostructured metal films under the Kretschmann configuration," J. Appl. Phys. **106**, 124314 (2009).
5. M. N. Velasco-Garcia, "Optical biosensors for probing at the cellular level: a review of recent progress and future prospects," Semin. Cell. Dev. Biol. **20**, 27–33 (2009).
6. H. Raether, *Surface Plasmons on Smooth and Rough Surfaces and on Gratings* (Springer Verlag, 1988).
7. E. Wijaya, C. Lenaerts, S. Maricot, J. Hastanin, S. Habraken, J.-P. Vilcot, R. Boukherroub, and S. Szunerits, "Surface plasmon resonance-based biosensors: from the development of different SPR structures to novel surface functionalization strategies," Curr. Opin. Solid State Mater. Sci. **15**, 208–224 (2011).
8. E. Ozbay, "Plasmonics: merging photonics and electronics at nanoscale dimensions," Science **311**, 189–193 (2006).
9. J. r. H. Hana Šípová, "Surface plasmon resonance sensing of nucleic acids: a review," Anal. Chim. Acta **773**, 9–23 (2013).
10. E. Petryayeva and U. J. Krull, "Localized surface plasmon resonance: nanostructures, bioassays and biosensing—a review," Anal. Chim. Acta **706**, 8–24 (2011).
11. S. Roh, T. Chung, and B. Lee, "Overview of the characteristics of micro- and nano-structured surface plasmon resonance sensors," Sensors **11**, 1565–1588 (2011).
12. P. G. Kik, *Surface Plasmon Nanophotonics* (Springer, 2007).
13. M. Zourob, *Optical Guided-Wave Chemical and Biosensors I* (Springer, 2010).
14. A. Z. K. Md. Saiful Islam, "Simulation and analysis of a sub-wavelength grating based multilayer surface plasmon resonant biosensor," J. Lightwave Technol. **31**, 1388–1398 (2013).
15. S. H. Choi, S. J. Kim, and K. M. Byun, "Characteristics of light emission from surface plasmons based on rectangular silver gratings," Opt. Commun. **283**, 2961–2966 (2010).
16. K. H. Yoon, M. L. Shuler, and S. J. Kim, "Design optimization of nano grating surface plasmon resonance sensors," Opt. Express **14**, 4842–4849 (2006).
17. K. Kim, S. J. Yoon, and D. Kim, "Nanowire-based enhancement of localized surface plasmon resonance for highly sensitive detection: a theoretical study," Opt. Express **14**, 12419–12431 (2006).
18. W. K. Jung and K. M. Byun, "Fabrication of nanoscale plasmonic structures and their applications to photonic devices and biosensors," Biomed. Eng. Lett. **1**, 153–162 (2011).
19. K. M. Byun, M. L. Shuler, S. J. Kim, S. J. Yoon, and D. Kim, "Sensitivity enhancement of surface plasmon resonance imaging using periodic metallic nanowires," J. Lightwave Technol. **26**, 1472–1478 (2008).
20. S. J. Yoon, K. M. Byun, D. Kim, and S. J. Kim, "Experimental study of sensitivity enhancement in surface plasmon resonance biosensors by use of periodic metallic nanowires," Opt. Lett. **32**, 1902–1904 (2007).
21. X. D. Hoa, A. G. Kirk, and M. Tabrizian, "Enhanced SPR response from patterned immobilization of surface bioreceptors on nano-gratings," Biosens. Bioelectron. **24**, 3043–3048 (2009).
22. W. K. Jung, N.-H. Kim, and K. M. Byun, "Numerical study on an application of subwavelength dielectric gratings for high-sensitivity plasmonic detection," Appl. Opt. **51**, 4722–4729 (2012).
23. P. K. Maharana and R. Jha, "Chalcogenide prism and graphene multilayer based surface plasmon resonance affinity biosensor for high performance," Sens. Actuators B **169**, 161–166 (2012).
24. T. Kan, N. Tsujiuchi, E. Iwase, K. Matsumoto, and I. Shimoyama, "Planar near-infrared surface plasmon resonance sensor with Si prism and grating coupler," Sens. Actuators B **144**, 295–300 (2010).
25. J. L. Volakis, A. Chatterjee, and L. C. Kempel, *Finite Element Method for Electro-Magnetics* (IEEE, 1998).
26. J. Jin, *The Finite Element Method in Electromagnetics* (Wiley, 2002).
27. P. Monk, *Finite Element Methods for Maxwell's Equations* (Oxford University, 2003).
28. P. Berini and R. Buckley, "On the convergence and accuracy of numerical mode computations of surface plasmon waveguides," J. Comput. Theor. Nanosci. **6**, 2040–2053 (2009).
29. E. D. Palik, *Handbook of Optical Constants of Solids* (Academic, 1998).
30. K. M. Byun and S. H. Choi, "Investigation on an application of silver substrates for sensitive surface plasmon resonance imaging detection," J. Opt. Soc. Am. A **27**, 2229–2236 (2010).
31. Y. L. Kim, S. H. Choi, and K. M. Byun, "Graphene-on-silver substrates for sensitive surface plasmon resonance imaging biosensors," Opt. Express **19**, 458–466 (2011).
32. K. M. Byun, D. Kim, and S. J. Kim, "Investigation of the profile effect on the sensitivity enhancement of nanowire-mediated localized surface plasmon resonance biosensors," Sens. Actuators B **117**, 401–407 (2006).
33. M. P. A. J. Homola, "Surface plasmon resonance: approaching their limits," Opt. Express **17**, 16505–16517 (2009).
34. X. D. Hoa, A. G. Kirk, and M. Tabrizian, "Towards integrated and sensitive surface plasmon resonance biosensors: a review of recent progress," Biosens. Bioelectron. **23**, 151–160 (2007).
35. A. G. Kim, C. J. Alleyne, R. C. McPhedran, N.-A. P. Nicorovici, and D. Maystre, "Enhanced SPR sensitivity using periodic metallic structures," Opt. Express **15**, 8163–8169 (2007).